13th World Conference on Earthquake Engineering
Vancouver, B.C., Canada
August 1-6, 2004
Paper No. 183

DESIGN CRITERIA FOR SEISMIC ISOLATION RUBBER BEARINGS

Chamindalal Sujeewa LEWANGAMAGE[1], Masato ABE[2], Yozo FUJINO[3] and Junji YOSHIDA[4]

SUMMARY

Although seismic isolation rubber bearings in bridges and buildings have proven to be a very effective passive method for reducing earthquake-induced forces, a detailed mechanical modeling of rubber that is used in bearings under large strains has not been established. Hence, a 3D model of rubber failure and design criteria for safety evaluation of seismic isolation rubber bearings have not yet been developed. This paper presents: (1) modeling of rubber failure under large deformations; and (2) design criteria for safety evaluation of seismic isolation laminated rubber bearings (LRB). Failure tests of biaxial, uniaxial and simple shear were conducted for rubber materials under different rates of loading. The measured local strains at failure by image analysis were used to develop a failure model for rubber. Validity of the proposed failure model of rubber was verified; the model was introduced into a 3D finite element model of LRB, and it was compared with experimental results of bearings failure. Finally, design criteria, which can estimate ultimate failure characteristics of LRB are proposed for the safety evaluation, and were verified.

INTRODUCTION

Since the Northridge Earthquake of 1994 and the Hyogo-ken Nanbu Earthquake of 1995, the effectiveness of seismic isolation has been recognized widely, and many of the seismically isolated structures now in existence used seismic isolation laminated rubber bearings (LRB) as primary isolation devices. The behavior of these structures under earthquake loading is characterized by the mechanical behavior of LRB under large deformations. It is important, therefore, to design seismically isolated structures with a full understanding of the mechanical behavior of LRB at failure. However, a 3D model of rubber failure, and design criteria for safety evaluation have not yet been developed.

Failure of the rubber is an important aspect to be considered in the design of LRB. However, a detailed mechanical modeling of rubber failure under large strains has not been fully established. Because of the difficulties in measuring large strain near the failure of rubber materials, "failure of rubber" is not clearly understood [1] and consequently no failure models have been developed. Kawabata [2] has studied

---

[1] Ph.D. Student, The University of Tokyo, Tokyo, Japan. Email: sujeewa@bridge.t.u-tokyo.ac.jp
[2] Associate Professor, The University of Tokyo, Tokyo, Japan. Email: masato@bridge.t.u-tokyo.ac.jp
[3] Professor, The University of Tokyo, Tokyo, Japan. Email: fujino@bridge.t.u-tokyo.ac.jp
[4] Assistant Professor, University of Yamanashi, Kofu, Japan. Email: jyoshida@ccn.yamanashi.ac.jp

fracture of rubber like polymer materials under biaxial stress field. Our previous studies [3, 4] has presented with large strains measurement technique of rubber by image analysis.

As solutions to the above problems, this paper presents: (1) modeling of rubber failure under large deformations; and (2) design criteria, which can estimate ultimate failure characteristics of LRB for safety evaluation. Seismic isolation LRB and two different rubber materials are selected for the study.

EXPERIMENTAL

Series of failure tests were conducted for rubber material from two different companies (*Types **A** and **B***). Both companies have provided natural rubber materials made with shear modulus equal to 0.98 MPa. Basically, for rubber materials, uniaxial, biaxial and simple shear failure tests were performed. The details of the tests are discussed as follows.

Material tests of '*Type-A*' rubber

Simple shear and uniaxial tension tests were conducted. Figure 1 shows the JIS K 6301 standard tension specimen [5] and special shear specimen [6] that were used for the study.

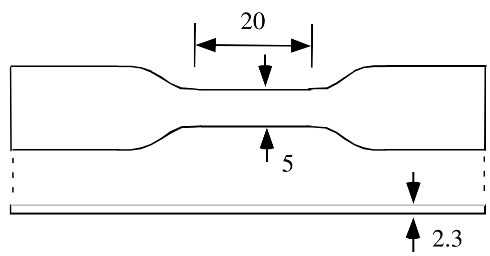

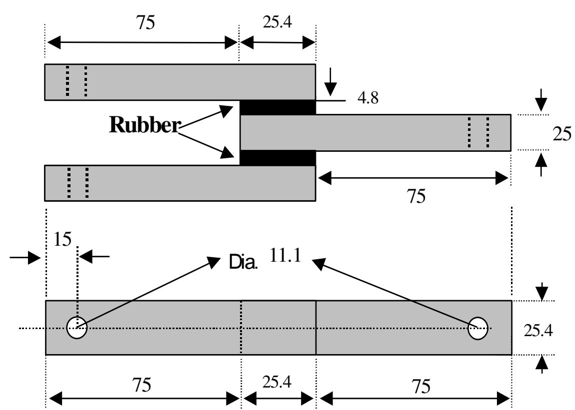

Figure 1. Test specimens: (a) tension; (b) shear

Both tests were conducted under monotonic loading until failure under different loading rates. Detailed descriptions of the tests are given in Table 1. Test setups are shown in Figure 2. The image analysis algorithms used to estimate failure strain are discussed in ref. [3].

Table 1. Material test descriptions (*Type-A* rubber)

	Uniaxial tension	Simple shear
Type of rubber (Shear modulus in Mpa)	Natural (0.98)	Natural (0.98)
Loading velocity [mm/sec]	1.33, 2.67, 5.33	0.024, 0.048, 0.24, 0.48, 0.96
Strain rate [%/sec]	-	0.50, 1.0, 5.0, 10, 20
Specimen tested per case	4	2
Temperature [°C]	20~25	12~14

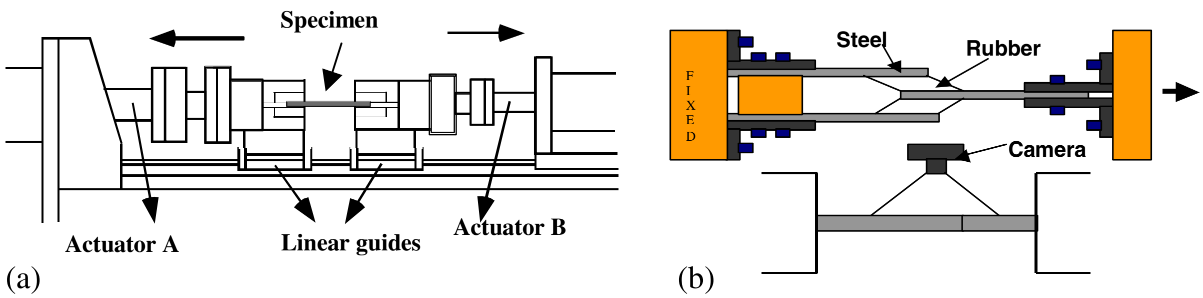

Figure 2. Schematic of test setups: (a) tension; (b) shear

Material tests of '*Type-B*' rubber

Biaxial and uniaxial failure tests were conducted. Specimens used for biaxial tests and uniaxial tests are shown in the Figures 3 and 4 respectively.

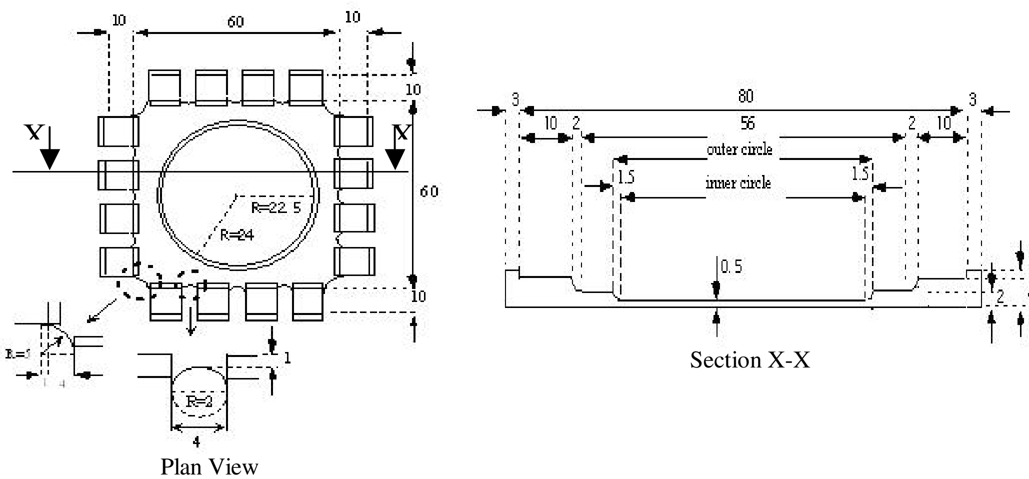

Figure 3. Detailed drawings (Biaxial specimen) – All dimensions in mm.

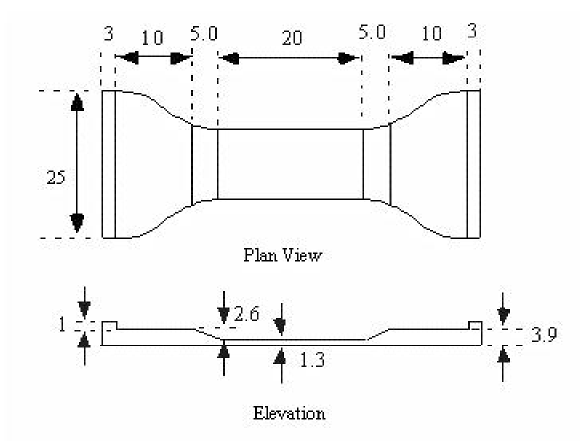

Figure 4. Detailed drawings (Uniaxial tension specimen)- All dimensions in mm.

The central parts of the biaxial test specimen and uniaxial test specimen are thinner compared to outer part (fixing part) to make sure that the failure will occur within the specimens. All the tests were conducted under monotonic loading until failure with different loading rates. Under biaxial tests series, equi-biaxial (average extension ratios kept constant in both direction) and strip biaxial (average extension ratio is constant in one direction) tests were performed. Extension ratio is defined as ratio between deformed length and original length in given direction. A line diagram for biaxial test is shown in Figure 5. Detailed descriptions of the tests are given in Table 2.

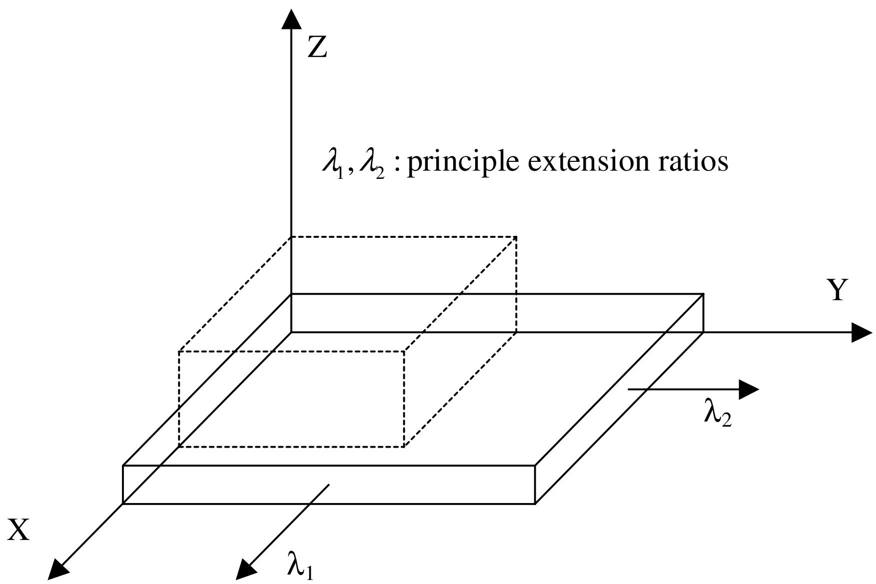

Figure 5. A line diagram for biaxial deformation

Table 2. Material test descriptions (*Type-B* rubber)

	Uniaxial tension	Biaxial (Strip/equi-biaxial)
Type of rubber (Shear modulus in Mpa)	Natural (0.98)	Natural (0.98)
Loading velocity [mm/sec]	0.2, 2, 20	0.2, 2.0, 20
Specimen tested per case	3~5	3~5
Temperature [°C]	20~25	20~25

Test setups are shown in Figure 6. Images of deformation of the specimens were taken using a CCD camera. Figure 7 shows a biaxial specimen at un-deformed stage and after deformation under equi-biaxial test. As shown in Figure 6a, deformation of the initially drawn gird on the specimen was traced using image analysis algorithms (Template matching). Here, a grid itself is used as a template. Template matching algorithms are fully discussed in [3,4].

Bearing tests

Two '***Type-A***' rubber laminated bridge bearings were tested under combined compressive and shear loadings. First, 1471 KN [5.88 MPa] compressive load was applied, then, shear displacement was given with a velocity 1mm/sec until failure. However, one bearing failed due to rubber-steel bond failure while the other failed by rubber failure. The details of the tested bearing that failed by rubber failure are given in Table 3 and its failure displacement was 312 mm. All the details of the experimental results have been discussed in ref. [3].

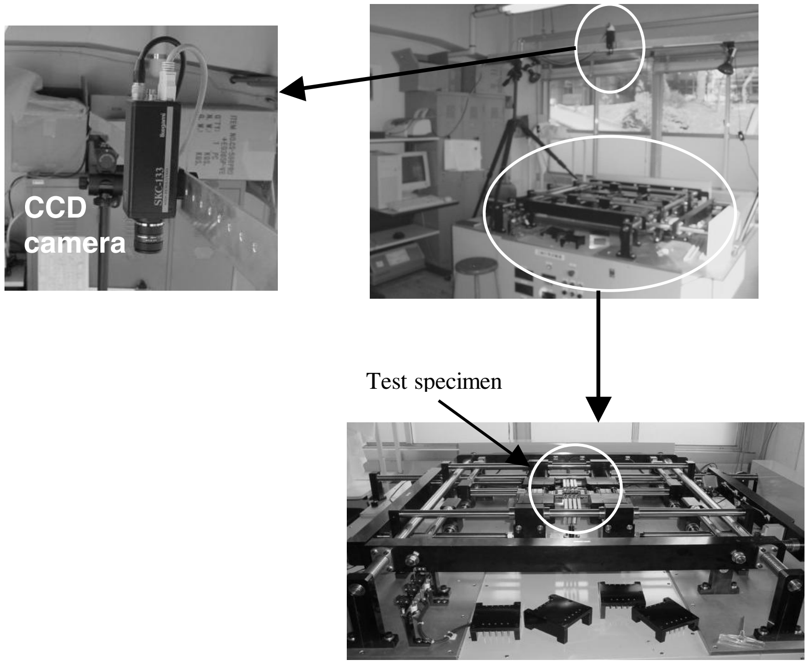

Figure 6. Test setup for biaxial/uniaxial tests

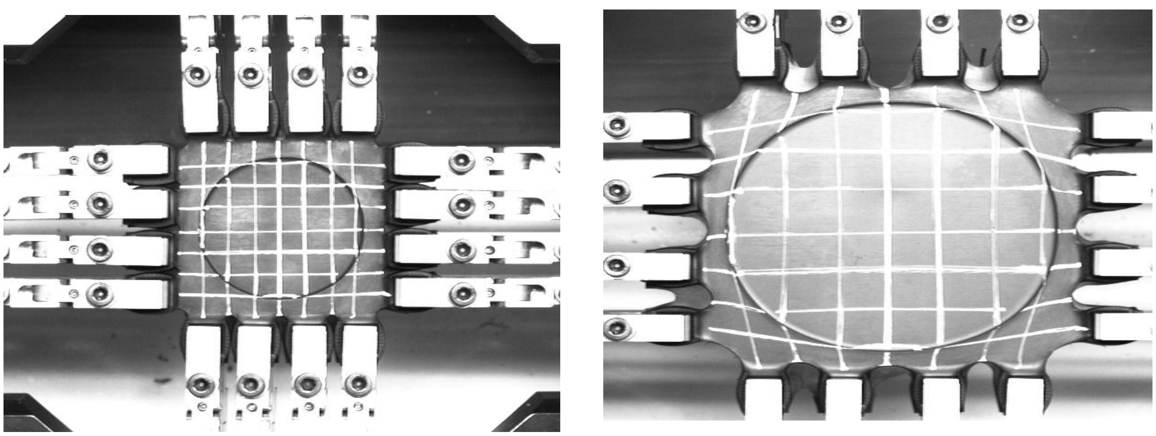

(a) (b)

Figure 7. Biaxial test specimen: (a) un-deformed; (b) deformed

Table 3. Details of tested LRB

Description	Values
Shear modulus of rubber [MPa]	0.98
Plan dimensions [mm]	500×500
A rubber layer thickness [mm]	30
Number of rubber layers	3
Steel type, thickness of a layer [mm]	SS 400, 10

TESTS RESULTS

Material tests of '*Type- A*' rubber

For the simple shear tests, the image analysis algorithms were applied to measure strain field [3]. Finally, local shear strain components at the failure points were calculated; these are shown in Figure 8. Failure shear strain variation is about ±10% to the average (443%) for different rates of loading. From experimental results, the shear strain and lateral strain component variation in rubber materials clearly indicated that strain localization occurred at the large deformation range before failure.

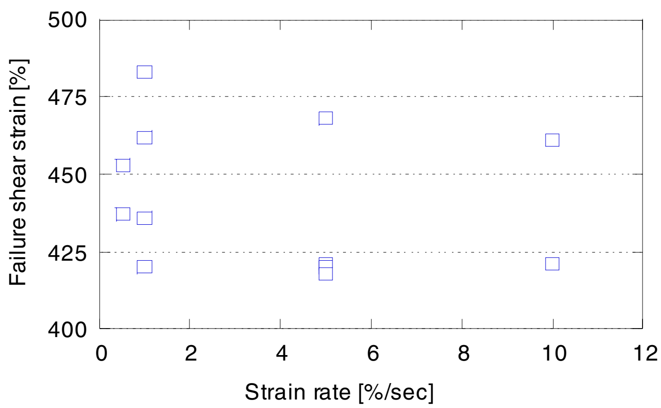

Figure 8. Shear strains at failure (*Type-A* rubber)

In the uniaxial tensile tests, deformations of the center part of the specimens were considered, because failure mostly occurred at the center part. Figure 9 shows extension ratios at failure. The maximum variation of failure extension ratio is about ±8% to the average (4.99) for different velocities of loading. The extension ratio is defined by the ratio between the deformed length and the un-deformed length of the center part (straight part) of the specimen.

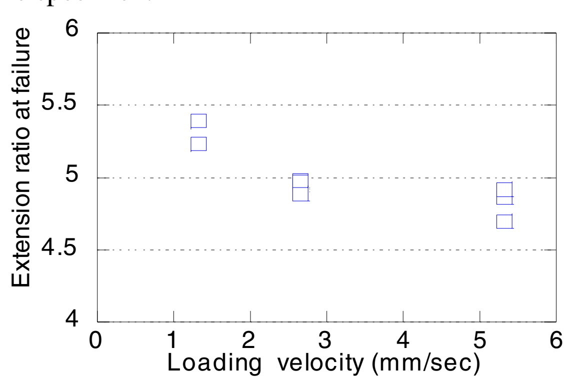

Figure 9. Extension ratio's at failure (*Type-A* rubber)

Material tests of '*Type-B*' rubber

The image analysis algorithms were applied to measure the strain field at failure. Using the grids deformations at failure, average extension ratios at failure were measured. Figure 10 shows extension ratios at failure for both biaxial and uniaxial tests. The failure results show that the extension ratios at failure have considerable variation (±8%) to its mean even for same stain rate.

In all the shear, biaxial and uniaxial tests, the strain values at the failure have considerable variation, even for the same strain rate. This may be possibly due to small damages made during the manufacturing process of the specimens or due to use of different batches of rubber during the production of specimens. However, it is understood that there is no clear relation between loading rate and failure strain for the given range of loading (Figure 8, 9 and 10). It is thus reasonable to assume that failure is independent of strain rate of loading.

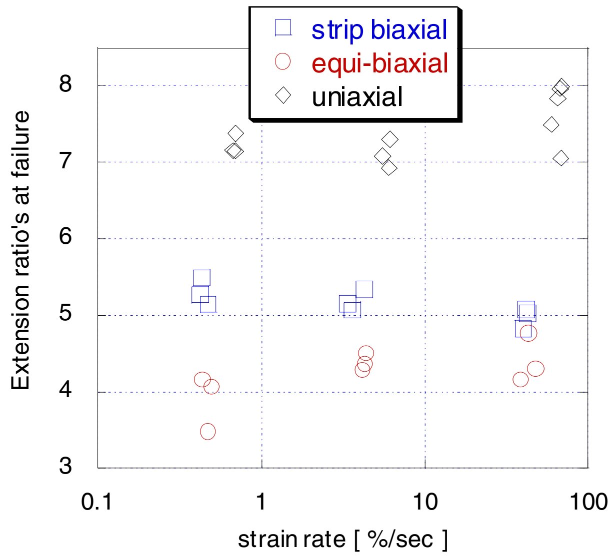

Figure 10. Results of failure tests of biaxial and uniaxial (*Type-B* rubber)

MODELING

Failure model for rubber

The use of this model allows a prediction of the critical strain under which rubber fails by crack initiation during virgin loading. Experimentally measured local maximum critical strain values at failure (at crack opening displacements) and extension ratios at failure (Figures 8, 9 and 10) are used in order to obtain such a model in which failure of rubber materials can be expressed in terms of its deformational characteristics. From the above-mentioned results of material tests, the failure of rubber material has been proven to be independent of the stain rate of loading. It has been observed experimentally that rubber material and rubber in bearings fail mostly at the edges of rubber layers due to development of large shear strains except in tensile deformation of rubber bearings, a fact which indicates that hydrostatic pressure does not affect to that failure mode. Therefore, it is assumed that failure behavior is isotropic and incompressible. Under these conditions, mathematical formulation for rubber failure under finite stains is developed. Two approaches has been considered; one is using failure extension ratio based approach which is similar approach done by Kawabata [2], and the other, more phenomenological based approach (invariants-based) which can be used easily in numerical modeling.

Extension ratio-based approach

In this approach, the extension ratios at failure can be used to develop a failure model. All the experimental results of biaxial, uniaxial and simple shear in both types of rubber are used to develop such a model. In "***Type-A***" rubber, simple shear test results are expressed in terms of equivalent strip biaxial results. The proposed failure model is given in Equation (1).

$$\lambda_1 \geq a(\lambda_2)^{-b} \; ; \lambda_1 \geq \lambda_2$$
$$\lambda_2 \geq a(\lambda_1)^{-b} \; ; \lambda_2 \geq \lambda_1 \qquad \textbf{(1a,b)}$$

where *a, b* are material constants and λ_1 and λ_2 are the principle extension ratios at failure respectively. The materials constants, which are estimated on the basis of the mean values of experimental results are shown in Table 4. Figure 11 shows graphical presentation of the model. It is clear that the model can reasonably express the failure behavior of both rubbers materials. When it compares with existing Kawabata's biaxial tests based model [2], Kawabata's model is highly over estimated the failure extension ratios.

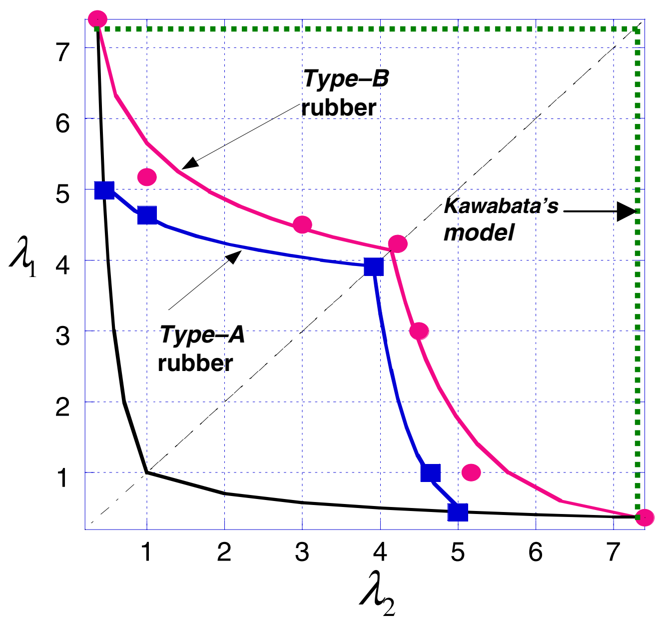

Table 4. Material constants

Rubber	*a*	*b*
Type-A	4.60	0.118
Type-B	5.65	0.218

Figure 11. Failure model for rubber (Extension ratios based)

Invariants-based approach

This is a similar approach that is made by authors in their earlier work [3]. phenomenologicaly, it can be defined that the strain energy density is constant at failure for a given rubber material, and can thus be called the break distortion energy density of that material. In a hyperelastic material, the strain energy density is a function of invariants of the right Cauchy green deformation tensor and the following form of strain energy density function is selected to fit the experimental results.

$$(\bar{I}_c - 3)(\bar{II}_c - 3) - \alpha_f (\bar{II}_c - 3)^2 \geq \beta_f \qquad \textbf{(2)}$$

where I_C, II_C are first and second invariants of the right Cauchy green deformation tensor, respectively, and α_f and β_f are the material constants which can be estimated from mean values of experimental results. Estimated material constants are shown in Table 5. A graphical presentation of the model is shown in Figure12. It is clear that the proposed criterion can averagely express the experimental failure behavior of rubber.

Constitutive model for rubber

The Authors has proposed a constitutive model for rubber to express its monotonic finite deformation behavior. Detailed discussion for the model is given in ref. [3]. The proposed strain energy density function for rubber is given in Equation (3).

$$W = c_4[1-\exp\{-c_5(I_C-3)\}] + c_1(I_C-3) + c_2(II_C-3)^K + \frac{c_3}{n+1}(I_C-3)^{n+1}(II_C-3)^{-m} \quad \textbf{(3)}$$

where c_i (i =1,2,3,4,5), m,n and k are material constants. Material constants estimated for '***Type-A***' rubber is given in Table 6.

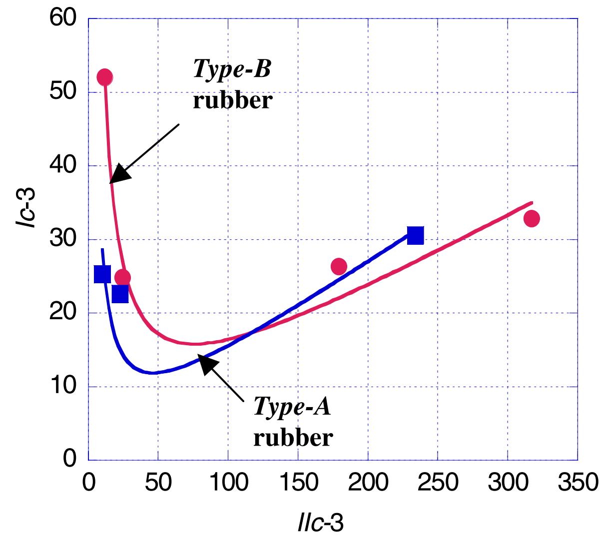

Figure 12. Failure model for rubber (Invariants-based)

Table 5. Material constants

Rubber	α_f	β_f
Type-A	0.1283	274.1
Type-B	0.1045	596.5

Table 6. Material constants

c_1 [N/mm^2]	2.90×10^{-1}
c_2 [N/mm^2]	6.00×10^{-4}
c_3 [N/mm^2]	1.75×10^{-1}
c_4 [N/mm^2]	1.00
c_5	8.00×10^{-2}
n	1.45
m	8.50×10^{-1}
K	3.03

Failure behavior of LRB

The validity of the proposed failure model is evaluated by applying it to the LRB. The invariant-based failure model is applied into finite element model [7] and the experimental failure test of a bearing was simulated. In the analysis, for the rubber material, the constitutive law proposed by the authors and the steel (SS400) constitutive law proposed by Chaboche [8] were used. The model was simulated by giving all the boundary conditions that were measured in the real experiment. Finally, FEM results are compared with the results of the failure experiment of LRB.

Figure 13 shows the contour plot of "A_f^2" by FEM when the deformation reached to the failure that was observed in the experiment of bearing failure. For this particular case, the relation between A_f and material constants of failure models can be obtained as follows

$$A_f = \sqrt{\frac{\beta_f}{1-\alpha_f}} \text{ or } a^2 \quad \textbf{(4)}$$

From the Figure 13, it is understood that the position of failure is the same as the failure position of the experiment. In addition, the value of "A_f" by FEM is 17.3 and it is within the range (17.1~23.5), which is obtained from the material experiments. Hence, the proposed failure criterion is proven to be valid for 3D modeling of failure behavior of seismic isolation LRB.

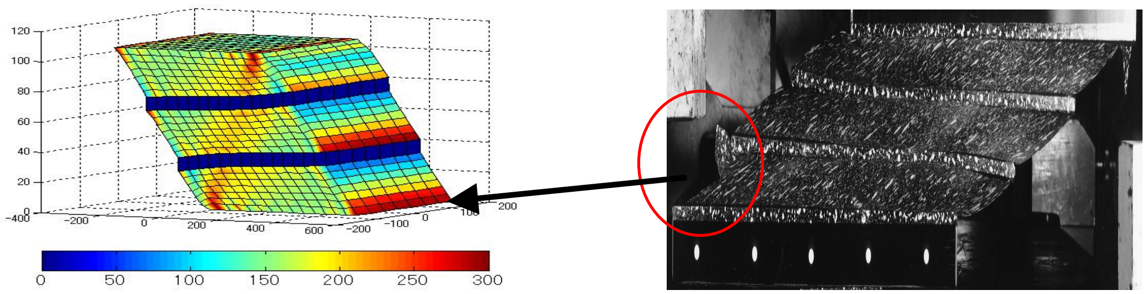

(a) (b)

Figure 13. 3D finite element modeling of failure behavior of LRB: (a) 3-D visualization of material conastant "A_f^2"; (b) Failure position of the bearing observed in the experiment.

DESIGN CRITERIA FOR SAFETY EVALUATION OF LRB

Analytical solution to calculate shear strains

Compressive and rotational deformation

Many tests have been conducted to investigate the behavior of elastomeric bearings in compression and rotations. Mori et al. [9] has reported some of the existing theories and empirical design formulas, and comparisons with the experimental results; he stated that there is a large difference between measured properties and the calculated ones. However, most of the theories developed so far are based on the work done by Rejcha [10] and similar solutions have been obtained to predict behavior of rubber bearings. It was also assumed that rubber is incompressible; however, Yoshida et al. [7] developed an analytical solution for compressive and rotational deformation of a rubber layer (Figure 14) by modifying the Rejcha's theory, assuming that rubber is slightly compressible.

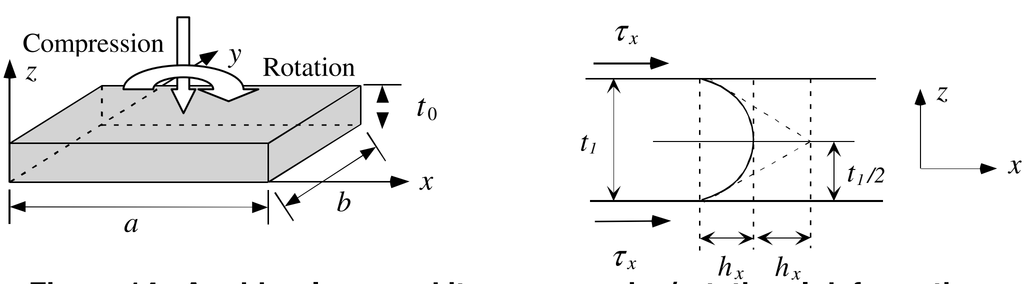

Figure 14. A rubber layer and its compressive/rotational deformation

Based on Yoshida's work, pressure field can be calculated for compressive and rotational deformation as given in Equations (5) and (6) respectively.

$$p_c = \sum_{n=1}^{\infty} \frac{q_n}{\alpha_n^2} \left\{ \frac{\sinh \alpha_n y + \sinh \alpha_n (b-y)}{\sinh \alpha_n b} - 1 \right\} \sin \frac{n\pi}{a} x \qquad \textbf{(5)}$$

where $$\alpha_n = \sqrt{\left(\frac{n\pi}{a}\right)^2 + \frac{3G}{\chi t_0^2}} \qquad \textbf{(5a)}$$

$$q_n = -\frac{24G}{n\pi t_0^3}(1-\cos n\pi)\Delta z \qquad \textbf{(5b)}$$

$$\chi = k/4 \qquad \textbf{(5c)}$$

where *(a, b)*, t_0, *G, k,* ΔZ, are respectively, cross sectional dimensions, thickness of the rubber layer, shear modulus, bulk modulus , total vertical displacement of the rubber layer.

$$p_R = \sum_{n=1}^{\infty} \frac{q_n}{\alpha_n^2} \left\{ \frac{\sinh \alpha_n y + \sinh \alpha_n (b-y)}{\sinh \alpha_n b} - 1 \right\} \sin \frac{n\pi}{a} x \qquad \textbf{(6)}$$

where $$q_n = -\frac{a\beta}{n\pi}(1+\cos n\pi) \qquad \textbf{(6a)}$$

$$\beta = -\frac{12G}{t_0^3}\tan\theta_R \cong -\frac{12G}{t_0^3}\theta_R \qquad \textbf{(6b)}$$

where θ_R is an angle of rotation of the upper plane of the rubber layer around the y–axis. Assuming that the shear deformation obeys Hook's law, the equilibrium equations for the rubber layer give the following formulas:

$$\frac{\partial p}{\partial x} = -8h_x \frac{G}{t_1^2} \qquad \textbf{(7)}$$

$$\frac{\partial p}{\partial y} = -8h_y \frac{G}{t_1^2} \qquad \textbf{(8)}$$

where *hx,hy* are projections of the parabolic deformation of the rubber layer on x-axis and y-axis respectively; and t_1 is rubber layer thickness after deformation (Figure 14).

Shear strain due to compression

Based on deformed geometry of the rubber layer (Figure 14), shear strain due to compression in x direction can be calculated as

$$\gamma_{cx} = \frac{4h_x}{t_1} \cong -\frac{t_0}{2G}\frac{\partial p_c}{\partial x} \qquad \textbf{(9)}$$

Theoretically, maximum shear strain due to compression can be calculated at the positions (x,y): *(0, b/2)* and *(a, b/2)*. They are equal in quantity and the positions where the shear stress value is maximum.

Shear strain due to rotation

Similar to shear strain due to compression, shear strain due to rotation can also be calculated as

$$\gamma_{rx} = \frac{4h_x}{t_1} \cong -\frac{t_0}{2G}\frac{\partial p_R}{\partial x} \qquad \textbf{(10)}$$

Shear strain due to shear

Maximum shear strain due to shear (γ_s) can be calculated in the usual way as

$$\gamma_s = \frac{\delta_s}{n_r} \quad \textbf{(11)}$$

where δ_s is lateral shear displacement and n_r is total rubber layer thickness.

Design criteria

The simplified criterion proposed using material tests and verified for bearing failure, can be applied to proposed design criteria for bearings for their safety evaluations. The failure criterion proposed for rubber can be combined with the analytical solutions, which can be used to calculate shear strain field of a rubber layer that is subjected to compressive deformations (Equation 9) or rotational deformations (Equation 10). The following load combinations are the most possible in rubber bearings; large shear strains are generated at the edges of the rubber layers at failure and it is known to be fail due to large shear strains.

Combined shear and compression

To obtain a simple relation to the failure, shear strain due to compression can be super-imposed with the shear strain due to shear because the total deformation gradient can be expressed simply by adding both deformation gradients together. Finally, the criterion can be used for the design as follows:

$$\max_{0\le x\le a,0\le y\le b}\{\gamma_s+\gamma_c(x,y)\}^2=\{\gamma_s+\gamma_c|_{x=0,y=b/2}\}^2\le A_f \quad \textbf{(12)}$$

$$\text{where}\quad \gamma_c|_{x=0,y=b/2}=\frac{12F_Z^{(B)}}{at_0^2}\left(\frac{C}{C_c}\right) \quad \textbf{(12a)}$$

$$C=\sum_{n=1}^{\infty}\frac{2}{\zeta_n^2}\left(1-\frac{1}{\cosh\zeta_n b/2}\right) \quad \textbf{(12b)}$$

$$C_c=\sum_{n=1}^{\infty}\frac{96Ga}{t_0^3\{(2n-1)\zeta_n\pi\}^2}\left\{b-\frac{2(1+e^{-2\zeta_n b})-4e^{-\zeta_n b}}{\zeta_n(1-e^{-2\zeta_n b})}\right\} \quad \textbf{(12c)}$$

$$\zeta_n=\sqrt{\left\{\frac{(2n-1)\pi}{a}\right\}^2+\frac{3G}{\chi t_0^2}} \quad \textbf{(12d)}$$

where $F_Z^{(B)}$ is applied compressive force. The material constant A_f can be estimated using the material constants of rubber failure models as follows.

$$A_f=\sqrt{\frac{\beta_f}{1-\alpha_f}}\ \text{or}\ a^2 \quad \textbf{(12e)}$$

Results comparison

The accuracy of the proposed design criterion (Equation 12) is evaluated by comparison with the results of the afore-mentioned failure experiment of bearing (δ_s = 312 mm, $F_Z^{(B)}$ = 1471 KN , k = 600 Mpa). When n = 1, A_f calculated using Equation (12) is 22.5 and it is in the upper limit of the range (17.1 ~ 23.5) that is obtained by material tests of rubber failure. The result implies validity of the proposed design criterion to predict failure of LRB under combined compressive and shear deformation. Figure 15 shows all the results comparison with invariant-based rubber failure model, and it shows reasonable agreement with results obtained from the material failure.

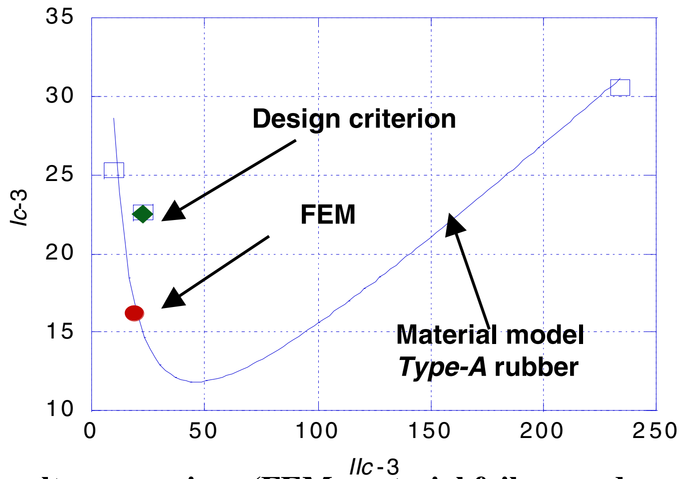

Figure 15. Results comparison (FEM, material failure and analytical solution)

Combined shear and rotation

Here, rotation is considered along the axis parallel to the y-axis through the center of the rubber bearing. Similarly to the above case, the maximum shear strain due to rotation can be superimposed with the shear strain due to shear. Finally, the design criterion can be used as follows:

$$\max_{0\le x\le a, 0\le y\le b} \left\{\gamma_s + \gamma_r(x,y)\right\}^2 = \left\{\gamma_s + \left|\gamma_r\,\Big|_{x=0,\,y=b/2}\right|\right\}^2 \le A_f \tag{13}$$

$$\text{where } \left|\gamma_r\,\Big|_{x=0,\,y=b/2}\right| = \frac{6M_R^{(B)}}{t_0^2}\left(\frac{C'}{C_R}\right) \tag{13a}$$

$$C' = \sum_{n=1}^{\infty}\frac{2}{\eta_n^2}\left(1-\frac{1}{\cosh\eta_n b/2}\right) \tag{13b}$$

$$C_R = \sum_{n=1}^{\infty}\frac{24Ga^3}{t_0^3(2n\pi\eta_n)^2}\left\{b-\frac{2(1+e^{-2\eta_n b})-4e^{-\eta_n b}}{\eta_n(1-e^{-2\eta_n b})}\right\} \tag{13c}$$

$$\eta_n = \sqrt{\left(\frac{2n\pi}{a}\right)^2+\frac{3G}{\chi t_0^2}} \tag{13d}$$

$$M_R^{(B)} = C_R\frac{\theta_R^{(B)}}{N} \tag{13e}$$

$$A_f = \sqrt{\frac{\beta_f}{1-\alpha_f}} \text{ or } a^2 \tag{13f}$$

where $M_R^{(B)}$ is the moment applied to the bearing.

Results comparison

Equation (13) cannot be verified due to unavailability of experimental results. However, the mode of failure is identical to combined shear and compression.

CONCLUSIONS

This paper has presented detailed modeling of failure of rubber materials under large deformations and its application to model the 3D failure behavior of seismic isolation LRB. Finally, design criteria have proposed for safety evaluation of LRB, and were verified. In addition, the following remarks also can be drawn from this paper.

- The proposed failure models for rubber can be applied to estimate the failure behavior of different types of rubber materials.
- Proposed 3D model to estimate the failure of LRB shows reasonable agreement with experimental results.
- Deign criterion proposed for safety evaluation of LRB under combined compression and shear deformation can be applied to estimate its failure behavior well.
- Further experiments are being conducted to investigate failure behavior of LRB under tensile and fatigue loadings.
- Design criteria proposed for safety evaluation of LRB could be implemented in design codes after verifying it by performing several full-scale tests.

ACKNOWLEDGMENTS

The authors wish to acknowledge Nippon Chuzo Company and Japan Association of Rubber Bearings for providing testing materials. This research is co-supported by the Ministry of Education, Sports, Science and Culture, Japan.

REFERENCES

1. Stanton JF, Roeder CW. “Elastomeric bearing design, construction and material.” National Cooperative Highway Research Program Report 248, Transportation Research Board, National Research Council, Washington, DC, 1982.
2. Kawabata S. “Fracture and mechanical behavior of rubber like polymers under finite deformation in biaxial stress field.” Journal of Macromolecular Science – Physics 1973; B8 (3-4): 605-630.
3. Lewangamage CS, Abe M, Fujino Y, Yoshida J. “ Strain field measurements of rubber by image analysis and design criteria for laminated rubber bearings.” Journal of Earthquake Engineering and Structural Dynamics 2004; 33 (4): 445-464.
4. Yoshida J, Abe M, Fujino Y, Lewangamage CS. “Measurement method for continua by image processing.” *Journal of Structural Engineering;* ASCE (In press).
5. Japanese Industrial Standards Committee. JIS-K-6301, 1983.
6. American Association of State Highway and Transportation Officials (AASHTO) “Guide specification for seismic isolation design.” Washington, DC, 1999.
7. Yoshida J, Abe M, Fujino Y, Watanabe H. “Three dimensional finite element analysis for high damping rubber bearings.” Journal of Engineering Mechanics 2004; ASCE, 130(5).
8. Chaboche LJ. “Constitutive equation for cyclic plasticity and cyclic viscoplasticity.” International Journal of Plasticity 1989; **5**:247-301.
9. Mori A, Carr AJ, Cooke N, Moss PJ. “Compression behaviour of bridge bearings used for seismic isolation.” Engineering structures 1996; 18(5): 351-362.
10. Rejcha C. “Design of elastomer bearings.” PCI Journal 1964; 62-78.
11. Treloar LRG. “The physics of rubber elasticity.” 3rd edn, Oxford: Clarendon press, 1975.